

A Mixed-Integer Conic Program for the Moving-Target Traveling Salesman Problem based on a Graph of Convex Sets

Allen George Philip¹, Zhongqiang Ren², Sivakumar Rathinam¹ and Howie Choset²

Abstract—This paper introduces a new formulation that finds the optimum for the Moving-Target Traveling Salesman Problem (MT-TSP), which seeks to find a shortest path for an agent, that starts at a depot, visits a set of moving targets exactly once within their assigned time-windows, and returns to the depot. The formulation relies on the key idea that when the targets move along lines, their trajectories become convex sets within the space-time coordinate system. The problem then reduces to finding the shortest path within a graph of convex sets, subject to some speed constraints. We compare our formulation with the current state-of-the-art Mixed Integer Conic Program (MICP) solver for the MT-TSP. The experimental results show that our formulation outperforms the MICP for instances with up to 20 targets, with up to two orders of magnitude reduction in runtime, and up to a 60% tighter optimality gap. We also show that the solution cost from the convex relaxation of our formulation provides significantly tighter lower bounds for the MT-TSP than the ones from the MICP.

I. INTRODUCTION

Given a set of stationary targets and the cost of traversal between any pair of these targets, the classical Traveling Salesman Problem (TSP) seeks to find the shortest tour for an agent such that it visits all the targets exactly once. The TSP is one of most fundamental problems in combinatorial optimization, with several applications including unmanned vehicle planning [1]–[4], transportation and delivery [5], monitoring and surveillance [6], [7], disaster management [8], precision agriculture [9], and search and rescue [10], [11]. In this paper, we consider the generalization of the TSP, where the targets follow some predefined trajectories, and also have associated time-windows during which they need to be visited. The objective is to minimize the distance traversed by the agent. We refer to this generalization as the Moving-Target TSP or MT-TSP for short. In the literature, we find different variants of the MT-TSP, motivated by practical applications such as defending an area from oncoming hostile rockets or Unmanned Aerial Vehicles [12]–[14], monitoring and surveillance [15]–[18], resupply missions with moving targets [12], dynamic target tracking [19], and industrial robot planning [20].

The speed of the targets are generally assumed to be no greater than the agent’s maximum speed [12]. When the

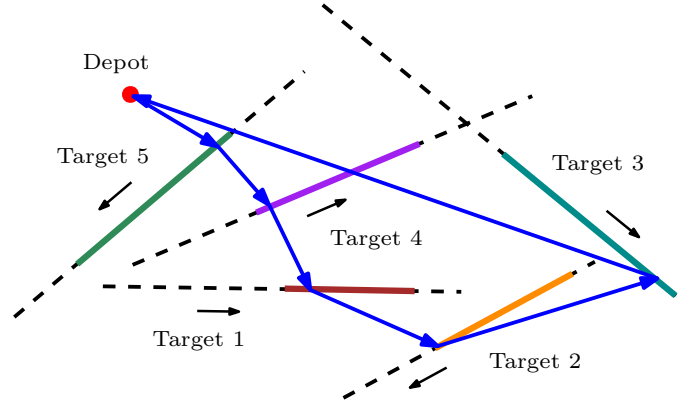


Fig. 1. A feasible solution to an example instance of the MT-TSP where 5 targets move along lines. The agent’s tour is given in blue, and the part of each target’s trajectory corresponding to its time-window where they can be visited by the agent are given by colored solid segments.

speed of all the targets reduces to 0, the MT-TSP reduces to the classical TSP. Hence, MT-TSP is NP-hard. Currently, the literature presents exact and approximation algorithms for some very restricted cases of the MT-TSP variants where the targets move in the same direction with the same speed [20], [21], move along the same line [12], [22], or move along lines through the depot, towards or away from it [12]. Several heuristic based approaches have also been introduced in the literature [15]–[17], [19], [23]–[27] that finds feasible solutions, but gives no information on how far they are from the optimum.

The objective of this paper is to find exact solutions to a less restricted case of the MT-TSP where the targets move along lines, with fixed speeds (refer to Fig. 1). Currently, the only approach that does this, is the MICP (specifically, a mixed-integer SOCP) introduced in [14]. Hence, we use this formulation as a baseline, and introduce an alternative formulation that finds the optimum for the MT-TSP. This formulation relies on the key idea that when the targets move along lines, their trajectories become convex sets within the space-time coordinate system. This reduces the MT-TSP to a problem of finding the shortest agent path within a graph of convex sets [28], subject to some additional speed constraints. We prove the validity of our approach, and provide computational results to corroborate the performance of our formulation. We find that our approach vastly outperforms the

¹Allen George Philip and Sivakumar Rathinam are with the Department of Mechanical Engineering, Texas A&M University, College Station, TX 77843-3123. Emails: {y262u297, srathinam}@tamu.edu

²Zhongqiang Ren and Howie Choset are at Carnegie Mellon University, 5000 Forbes Ave., Pittsburgh, PA 15213, USA. Emails: {zhongqir, choset}@andrew.cmu.edu

baseline and scales much better when increasing the time-window duration and the number of targets, achieving up to a two orders of magnitude faster average runtime and up to a 60% improvement in the average optimality gap. We also show that our formulation has a much stronger convex relaxation than the baseline, which can be used to find lower-bounds to the MT-TSP with significantly lower computational burden.

II. PROBLEM DEFINITION

All the targets and the agent move in a 2D (x, y) plane. Let $V_{tar} := \{1, 2, \dots, n\}$ denote the set of n moving targets, and let s be the depot. Without loss of generality, we make a copy of the depot and refer to it as s' and require the agent to return to s' at the end of its tour. Let $V := V_{tar} \cup \{s, s'\}$. Given a node $i \in V$, the time-window associated with that node is denoted by $[\underline{t}_i, \bar{t}_i]$. The (x, y) position occupied by node i at time \underline{t}_i and \bar{t}_i is denoted by $(\underline{p}_{i,x}, \underline{p}_{i,y})$ and $(\bar{p}_{i,x}, \bar{p}_{i,y})$ respectively, and the velocity coordinates of node i is denoted by $(v_{i,x}, v_{i,y})$. Note that we fix $\underline{t}_s = \bar{t}_s = 0$ since the agent tour starts at time 0. In addition, we fix $\underline{t}_{s'} = 0$ and $\bar{t}_{s'} = T$ where T is the time-horizon, so that the agent is free to complete the tour at any time within $[0, T]$. Also note that the velocity of the depot, $(v_{s,x}, v_{s,y})$ and the velocity of the depot's copy, $(v_{s',x}, v_{s',y})$ are fixed to be $(0, 0)$ since they are stationary. We say that the agent visits a moving target (say i) if there is a time instant in $[\underline{t}_i, \bar{t}_i]$ when the position of the agent coincides with the position of the target i . Any feasible tour for the agent will start from s , visit each target in V_{tar} exactly once and return to s' . The objective of the MT-TSP is to find a feasible tour for the agent such that the distance traveled by the agent along the tour is minimized.

III. MICP FOR MT-TSP

This section presents the current state-of-the-art MICP formulation introduced in [14] for the MT-TSP. The formulation in [14] is slightly modified for this paper so that the agent tour starts at s and ends at s' . To proceed further, we first construct a directed graph (V, E) where the edges in E are added as follows: from node s to all the nodes in V_{tar} , from each node in V_{tar} to every other node in V_{tar} , and finally, from every node in V_{tar} , to node s' .

Next, we define the decision variables for this formulation. For each node $i \in V$, the real variable t_i represents the time at which the agent visits i . For each edge $e = (i, j) \in E$, variable $y_e \in [0, 1]$ represents the flow through that edge. In a binary program, $y_e \in \{0, 1\}$, and it represents the decision of whether or not edge e is chosen. We will consider y_e as a binary variable unless otherwise stated. The auxiliary variable $\tilde{l}(p_i, p_j) \geq 0$ represents $\|p_j - p_i\|y_e$ where for some node i , $p_i = (p_{i,x}, p_{i,y})$ describes the position of that node at time t_i . The formulation also introduces other real auxiliary variables, $l_x(p_i, p_j)$ and $l_y(p_i, p_j)$ which represents $p_{j,x} - p_{i,x}$ and $p_{j,y} - p_{i,y}$ respectively, and finally $\tilde{l}(p_i, p_j) \geq 0$ which will be used to define the second-order cone constraints.

We also note that there is a parameter R which denotes the length of the diagonal of the square area that contains the

depot and all the target trajectories. The fact that the Euclidean norm of any line segment within the square area cannot exceed R will be used in formulating one of the constraints in the formulation. Now, the MICP formulation for the MT-TSP is as follows:

$$\min \sum_{e=(i,j) \in E} \tilde{l}(p_i, p_j) \quad (1)$$

$$\sum_{e \in E_s^{out}} y_e = 1 \quad (2)$$

$$\sum_{e \in E_{s'}^{in}} y_e = 1 \quad (3)$$

$$\sum_{e \in E_i^{in}} y_e = 1, \quad \forall i \in V_{tar} \quad (4)$$

$$\sum_{e \in E_i^{in}} y_e = \sum_{e \in E_i^{out}} y_e, \quad \forall i \in V_{tar} \quad (5)$$

$$\underline{t}_i \leq t_i \leq \bar{t}_i, \quad \forall i \in V \quad (6)$$

$$l_x(p_i, p_j) - ((\underline{p}_{j,x} + t_j v_{j,x} - \underline{t}_j v_{j,x}) - (\underline{p}_{i,x} + t_i v_{i,x} - \underline{t}_i v_{i,x})) = 0, \quad \forall e = (i, j) \in E \quad (7)$$

$$l_y(p_i, p_j) - ((\underline{p}_{j,y} + t_j v_{j,y} - \underline{t}_j v_{j,y}) - (\underline{p}_{i,y} + t_i v_{i,y} - \underline{t}_i v_{i,y})) = 0, \quad \forall e = (i, j) \in E \quad (8)$$

$$\tilde{l}(p_i, p_j) \leq v_{max}(t_j - t_i + T(1 - y_e)), \quad \forall e = (i, j) \in E \quad (9)$$

$$\tilde{l}(p_i, p_j) = \tilde{l}(p_i, p_j) + R(1 - y_e), \quad \forall e = (i, j) \in E \quad (10)$$

$$(l_x(p_i, p_j))^2 + (l_y(p_i, p_j))^2 \leq (\tilde{l}(p_i, p_j))^2, \quad \forall e = (i, j) \in E \quad (11)$$

The objective (1) is to minimize the total tour length of the agent. The condition that the agent departs from the depot once, and arrives at the depot's copy once, is described by (2) and (3) respectively. The constraints, (4) ensures that each target is visited exactly once by the agent, and the flow conservation for all the target nodes are ensured by (5). Constraints (2) to (5) are fundamental to the MT-TSP, and ensures a valid agent path that starts at the depot, visits all the targets exactly once, and returns to the depot. Hence, these constraints will be repeated for all the formulations in this article. The condition requiring the agent to visit each node within its time-window is given by (6), and the definitions of the auxiliary variables $l_x(p_i, p_j)$ and $l_y(p_i, p_j)$ are captured through (7) and (8), respectively.

Now, we will explain the big- M constraints, (9), and (10), for each edge $e = (i, j) \in E$. First, consider the time-feasibility constraints, (9). These constraints describes the condition that if $y_e = 1$, then $\tilde{l}(p_i, p_j) \leq v_{max}(t_j - t_i)$. However, if $y_e = 0$, then no restrictions are placed on t_i and t_j . Second, consider the constraints, (10). With the help of (7), (8), these constraints, along with the second-order cone constraints, (11) describes the condition that $\tilde{l}(p_i, p_j) \geq \|p_j - p_i\|$ if $y_e = 1$. However, if $y_e = 0$, then $\tilde{l}(p_i, p_j)$ is free to take any value.

Although this formulation describes the MT-TSP well, it is computationally burdensome to solve in practice. Moreover, the presence of big- M constraints makes the convex relaxations weak. In this paper, we present a graph of convex sets (GCS) based MICP (MICP-GCS) that is significantly faster to solve, and provides much stronger relaxations. Prior to presenting this formulation, we will restate the current MICP as a biconvex problem. This will aid us in proving that an optimal solution to MICP-GCS, indeed provides an optimal solution to the MT-TSP.

IV. MICP ON THE GRAPH OF CONVEX SETS

A. Biconvex Formulation

In this section, we will restate the MICP for the MT-TSP as a biconvex, binary program. First, we present the decision variables for this formulation. For each node $i \in V$, we reuse the variable t_i from the MICP. In addition, we introduce real auxiliary variables, $p_{i,x}$ and $p_{i,y}$ that explicitly defines the (x, y) coordinates of p_i . For each edge $e = (i, j) \in E$, we use the variable y_e from before, as well as introduce real variables $z_{e,x}$, $z_{e,y}$, and $z_{e,t}$, corresponding to node i , and real variables $z'_{e,x}$, $z'_{e,y}$, and $z'_{e,t}$, corresponding to node j . Finally, we replace the variables $l_x(p_i, p_j)$, $l_y(p_i, p_j)$, and $\tilde{l}(p_i, p_j)$ from the MICP with real auxiliary variables $l_x(\tilde{z}_e, \tilde{z}'_e)$, $l_y(\tilde{z}_e, \tilde{z}'_e)$, and $l(\tilde{z}_e, \tilde{z}'_e) \geq 0$ respectively. Note that \tilde{z}_e and \tilde{z}'_e are notations describing $(z_{e,x}, z_{e,y})$ and $(z'_{e,x}, z'_{e,y})$ respectively. Also, notations z_e , and z'_e describes $(z_{e,x}, z_{e,t})$, and $(z'_{e,x}, z'_{e,t})$ respectively. The variable $\tilde{l}(p_i, p_j)$ introduced previously for each edge is not used in the biconvex formulation. This is because the big- M constraints are removed here. The formulation is presented below:

$$\min \sum_{e=(i,j) \in E} l(\tilde{z}_e, \tilde{z}'_e) \quad (12)$$

constraints (2), (3), (4), (5), (6)

$$p_{i,x} = \underline{p}_{i,x} + t_i v_{i,x} - \underline{t}_i v_{i,x}, \quad \forall i \in V \quad (13)$$

$$p_{i,y} = \underline{p}_{i,y} + t_i v_{i,y} - \underline{t}_i v_{i,y}, \quad \forall i \in V \quad (14)$$

$$l_x(\tilde{z}_e, \tilde{z}'_e) = (z'_{e,x} - z_{e,x}), \quad \forall e = (i, j) \in E \quad (15)$$

$$l_y(\tilde{z}_e, \tilde{z}'_e) = (z'_{e,y} - z_{e,y}), \quad \forall e = (i, j) \in E \quad (16)$$

$$l(\tilde{z}_e, \tilde{z}'_e) \leq v_{max}(z'_{e,t} - z_{e,t}), \quad \forall e = (i, j) \in E \quad (17)$$

$$(l_x(\tilde{z}_e, \tilde{z}'_e))^2 + (l_y(\tilde{z}_e, \tilde{z}'_e))^2 \leq (l(\tilde{z}_e, \tilde{z}'_e))^2, \quad \forall e = (i, j) \in E \quad (18)$$

$$z_e = (y_e p_i, y_e t_i), \quad z'_e = (y_e p_j, y_e t_j), \quad \forall e = (i, j) \in E \quad (19)$$

This formulation shares constraints (2) to (6) from the MICP. Constraints (13) and (14) describes variables $p_{i,x}$ and $p_{i,y}$. The nonconvexity of this program comes only from the bilinear constraints, (19). These constraints will be utilized to achieve the role satisfied by the big- M constraints in the MICP. First, notice how for each edge $e = (i, j) \in E$, when $y_e = 0$, (19) becomes $z_e = z'_e = (0, 0, 0)$. Consequently, (15), (16) becomes $l_x(\tilde{z}_e, \tilde{z}'_e) = l_y(\tilde{z}_e, \tilde{z}'_e) = 0$. However,

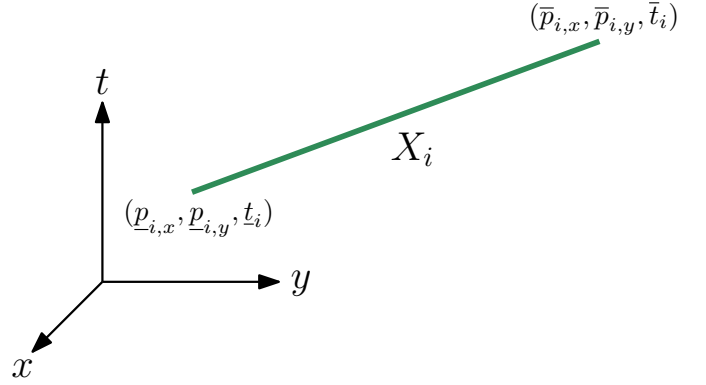


Fig. 2. The trajectory-segment that corresponds to the time-window of some node $i \in V$, is a line segment within the space-time coordinate system (x, y, t) . The set of all points in the line segment forms the convex set X_i .

when $y_e = 1$, (19) becomes $z_e = (p_i, t_i)$, $z'_e = (p_j, t_j)$ and consequently, (15), (16) becomes $l_x(\tilde{z}_e, \tilde{z}'_e) = p_{j,x} - p_{i,x}$, and $l_y(\tilde{z}_e, \tilde{z}'_e) = p_{j,y} - p_{i,y}$.

Now, consider (17). For each edge $e = (i, j) \in E$, when $y_e = 1$, these constraints become $l(\tilde{z}_e, \tilde{z}'_e) \leq v_{max}(t_j - t_i)$. However, when $y_e = 0$, we get $l(\tilde{z}_e, \tilde{z}'_e) \leq 0$, allowing t_i , and t_j to be free. Finally, consider (18). We see how these constraints with the help of (15), (16) becomes $l(\tilde{z}_e, \tilde{z}'_e) \geq \|p_j - p_i\|$ when $y_e = 1$, but allows $l(\tilde{z}_e, \tilde{z}'_e)$ to take any value when $y_e = 0$. Recall how the big- M constraints, (9), (10), and the constraints, (11) achieves the same role as (17) and (18) for $\tilde{l}(p_i, p_j)$. Hence, in the biconvex formulation, constraints (17) and (18) replaces constraints (9), (10) and (11) from the MICP, while establishing the relationship,

$$l(\tilde{z}_e, \tilde{z}'_e) = \tilde{l}(p_i, p_j) \quad (20)$$

From (20), we see how both the MICP and the biconvex formulation have the same optimal value. Moreover, we can recover an optimal tour for the MT-TSP from the solution of the biconvex program by picking all the edges with $y_e = 1$, and recovering the (p_i, t_i) for each node $i \in V$.

Now, we discuss the key idea behind the GCS-based MICP we introduce in this paper. Notice how the set of all $(p_{i,x}, p_{i,y}, t_i)$ that satisfy (6), (13), and (14) for each node $i \in V$ represents the trajectory-segment of that node within its time-window. These trajectory-segments are line segments when expressed within the (x, y, t) coordinate system as shown in the example illustration in Fig. 2. Hence, the trajectory-segment corresponding to each node i can be considered a convex set X_i corresponding to that node, and the agent is required to visit a point within X_i . This allows us to solve the MT-TSP by leveraging the ideas presented in [28], where the problem was to find the shortest paths in graphs of convex sets. To summarize, (6), (13), and (14), together can be represented using the following set of constraints.

$$(p_i, t_i) \in X_i, \quad \forall i \in V \quad (21)$$

Note that the nonconvexities which arise from the bilinear constraints makes solving the biconvex formulation very challenging. However in the next section, we will introduce our MICP-GCS formulation for the MT-TSP, that can be easily handled by standard solvers.

B. GCS-Based Mixed Integer Conic Program (MICP-GCS)

In this section, we present our new MICP-GCS formulation for the MT-TSP. First, we discuss the decision variables for this formulation. For each edge $e = (i, j) \in E$, we use the same variables $y_e, z_{e,x}, z_{e,y}, z_{e,t}, z'_{e,x}, z'_{e,y}, z'_{e,t}, l_x(\tilde{z}_e, \tilde{z}'_e), l_y(\tilde{z}_e, \tilde{z}'_e), l(\tilde{z}_e, \tilde{z}'_e)$ that we introduced in the biconvex formulation. Now, we present MICP-GCS:

$$\min \sum_{e=(i,j) \in E} l(\tilde{z}_e, \tilde{z}'_e) \quad (22)$$

constraints (2), (3), (4), (15), (16), (17), (18)

$$\sum_{e \in E_i^{in}} (z'_{e,t}, y_e) = \sum_{e \in E_i^{out}} (z_{e,t}, y_e), \quad \forall i \in V_{tar} \quad (23)$$

$$(z_e, y_e) \in \tilde{X}_i, (z'_e, y_e) \in \tilde{X}_j, \quad \forall e = (i, j) \in E \quad (24)$$

The MICP-GCS formulation differs from the the biconvex formulation in the following ways: The constraints, (23) are obtained by combining (5) with the additional constraints, $\sum_{e \in E_i^{in}} z'_{e,t} = \sum_{e \in E_i^{out}} z_{e,t}$ for each node $i \in V_{tar}$. These additional constraints ensures that the time at which the agent visits each target i will be equal to the time at which the agent departs from target i . Also, (21) which encapsulates (6), (13), (14), as well as the bilinear constraints, (19) are replaced by the constraints, (24). These constraints requires that for each edge $e = (i, j) \in E$, (z_e, y_e) and (z'_e, y_e) lies within the *perspective* of the convex sets X_i and X_j respectively. This is a compact way of representing the set of constraints for all the edges $e = (i, j) \in E$ as below:

$$y_e \underline{t}_i \leq z_{e,t} \leq y_e \bar{t}_i \quad (25)$$

$$y_e \underline{t}_j \leq z'_{e,t} \leq y_e \bar{t}_j \quad (26)$$

$$z_{e,x} - v_{i,x} z_{e,t} - y_e (\underline{p}_{i,x} - \underline{t}_i v_{i,x}) = 0 \quad (27)$$

$$z_{e,y} - v_{i,y} z_{e,t} - y_e (\underline{p}_{i,y} - \underline{t}_i v_{i,y}) = 0 \quad (28)$$

$$z'_{e,x} - v_{j,x} z'_{e,t} - y_e (\underline{p}_{j,x} - \underline{t}_j v_{j,x}) = 0 \quad (29)$$

$$z'_{e,y} - v_{j,y} z'_{e,t} - y_e (\underline{p}_{j,y} - \underline{t}_j v_{j,y}) = 0 \quad (30)$$

From an optimal solution to the MICP-GCS, we can recover an optimal agent tour for the biconvex program as follows: For each node $i \in V$, find the optimal (p_i, t_i) , using the following equations:

$$(p_i, t_i) = \sum_{e \in E_i^{in}} z'_e, \quad \forall i \in V \setminus \{s\} \quad (31)$$

$$(p_s, t_s) = \sum_{e \in E_s^{out}} z_e \quad (32)$$

C. Proof of Validity

In this section, we will show the correctness of the MICP-GCS formulation by proving the following theorem.

Theorem 1. *The optimal value of the MICP-GCS formulation is equal to the optimal value of the biconvex formulation for the MT-TSP. An optimal agent tour for the MT-TSP can be recovered from the solution of MICP-GCS by choosing $(p_i, t_i) \forall i \in V$ as shown in (31) and (32).*

Proof. Let E_{tour} be the set of all edges with $y_e = 1$, obtained from a solution to either of the two formulations. The constraints in both the formulations requires that the edges in E_{tour} forms a path that starts at s , visits all the target nodes once, and ends at s' , thereby forming an agent tour. For each edge $e \notin E_{tour}$, $z_e = z'_e = (0, 0, 0)$ for both the formulations. This is achieved by (19) in the biconvex formulation, and by (24) in the MICP-GCS formulation. Consequently, the cost addends corresponding to these edges becomes $l(\tilde{z}_e, \tilde{z}'_e) = 0$ for both formulations. Now, consider each edge $e = (i, j) \in E_{tour}$. In the biconvex formulation, (19) becomes $z_e = (p_i, t_i)$, $z'_e = (p_j, t_j)$. Additionally, (21) requires $(p_i, t_i) \in X_i$, $(p_j, t_j) \in X_j$. These two requirements are the same as saying $z_e \in X_i$, $z'_e \in X_j$, and for any two adjacent edges $e = (i, j)$ and $f = (j, k)$ in the agent tour, $z'_e = z_f$. In the MICP-GCS formulation, (24) becomes $z_e \in X_i$, $z'_e \in X_j$, and the additional flow requirement in (23) ensures that for any two adjacent edges $e = (i, j)$ and $f = (j, k)$ in the agent tour, $z'_e = z_f$. Therefore, the cost addends corresponding to edges $e \in E_{tour}$ becomes $l(\tilde{z}_e, \tilde{z}'_e)$ for both the formulations. Now, suppose that we have a solution to the MICP-GCS formulation. The (p_i, t_i) corresponding to each $i \in V$ can then be obtained as shown in (31) and (32) since it ensures $(p_i, t_i) = z_e$ and $(p_j, t_j) = z'_e$ for each $e = (i, j) \in E$ with $y_e = 1$. \square

V. NUMERICAL RESULTS

A. Test Settings and Instance Generation

All the tests were run on a laptop with an Intel Core I7-7700HQ 2.80GHz CPU, and 16GB RAM. The implementation was in Python 3.11.6, and both the MICP as well as MICP-GCS formulations were solved using Gurobi 10.0.3 optimizer. All the Gurobi parameters were set to their default values, except for *TimeLimit*¹, which was set to 1800.

A total of 80 instances were generated, 20 each for 5, 10, 15, and 20 targets. The instances were defined by the number of targets n , a square area of fixed size $S = 100$ units with corresponding diagonal length $R = \sqrt{2}S$, a fixed time-horizon $T = 150$, the depot location fixed at the center $(0, 0)$ of the square, and finally, a set of randomly generated linear trajectories corresponding to the n targets such that each target has a constant speed within $[0.5, 1]$ and is confined within the square area.

For each instance, we ran experiments where we varied two additional test parameters: the max agent speed v_{max} , and the

¹Limits the total time expended (in seconds).

time-windows corresponding to the targets. v_{max} was varied to be 4, 6, and 8 *unit/sec*, and the time-windows were varied to be of durations 25, 50, and 75 secs. The time-windows were selected such that a feasible solution could be found for all the generated instances, with all agent speed choices. To do this, we first randomly chose a sequence in which the agent visits the targets, and then found the quickest agent tour corresponding to that sequence by fixing the agent speed at its lowest choice (which is 4 *unit/sec*). If the time for the tour was more than T , we tried another random sequence. Otherwise, we took the times where the agent visited each target, and defined time-windows that contained these times. Note that when varying time-windows, we ensured that the time-window of duration 25 lies within the time-window of duration 50, which then lies within the time-window of duration 75, for each target.

B. Evaluating the Formulations

Given v_{max} , a time-window duration, and the formulation of choice, the solver is first run on all the 20 instances corresponding to a given number of targets. The optimality gap value from the solver for an instance is defined as $\frac{|z_P - z_D|}{|z_P|} \times 100$, where z_P is the primal (feasible) objective, and z_D is the dual (lower-bound) objective. Let % Gap denote the average of the smallest gap values output by the solver for all these instances, and let runtime be the average of the run-times output by the solver for all these instances.

C. Varying the Time-Window Duration

In this section, we consider the experiments where the time-window durations are varied. We do this by fixing the agent speed at 4, and solving all the instances for the time-window durations (25, 50, and 75). The results for this experiment are illustrated in Fig. 3, with (a), (b), and (c) corresponding to durations 25, 50, and 75 respectively. We observe that the problem becomes more challenging to solve for both the approaches as the number of targets increases. More importantly, this difficulty becomes more prominent as the time-window duration increases. The main advantage of MICP-GCS here is that it scales significantly better than the MICP against a larger number of targets and bigger time windows. We see this especially in the case of 15 targets where the % Gap always fully converges for the MICP-GCS and its runtime increases noticeably only with the largest time-window of duration 75, as compared to the MICP whose % Gap and runtime increases dramatically as the time-windows gets bigger. Note how the problem is challenging for both the approaches at 20 targets. However, we see that the % Gap or the runtime is always significantly improved for MICP-GCS, for all time-window durations in this case.

D. Varying the Agent Speed

In this section, we consider the second set of experiments where the agent maximum speed is varied. We do this by fixing the time-window duration at 50, and varying the agent max speed to 6, and 8. The results for this experiment is illustrated

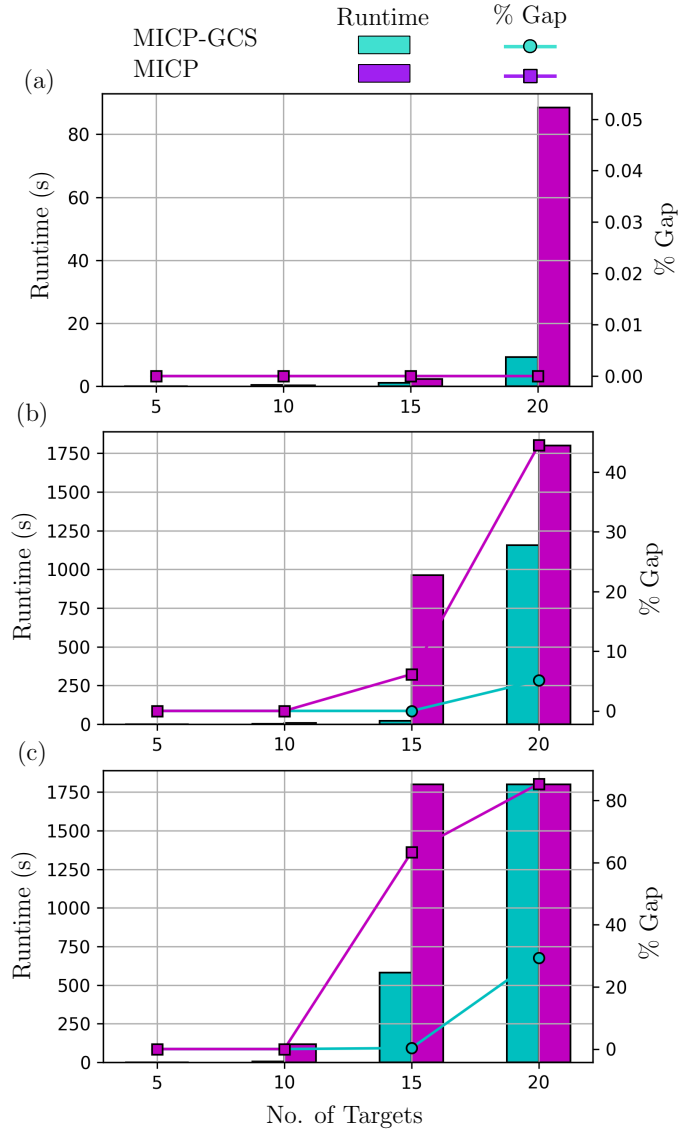


Fig. 3. Numerical results comparing runtime and % Gap of the MICP and MICP-GCS for a fixed max agent speed of 4, and varying time-window durations of 25 (a), 50 (b), and 75 (c). MICP-GCS scales significantly better than the MICP, when increasing the time-window duration, and number of targets. This can be seen especially for 15 targets in (b) and 10 targets in (c) where it runs up to 2 orders of magnitude faster while providing the same or better % Gap. Similarly, in the case of 15 targets in (c), and 20 targets in (b) and (c), MICP-GCS runs up to more than 1000 seconds faster, while providing a % Gap improvement within a 40-60 range.

in Fig. 4, with (a) and (b) corresponding to max speeds of 6 and 8 respectively. Note that Fig. 3 (b) gives the plot for when the agent max speed is 4. We observe that the plots look similar for all the three maximum agent speeds, with the runtime increasing slightly for both the approaches, and the % Gap getting slightly larger for the MICP, as the agent max speed is increased. This small increase in difficulty is believed to stem mostly from the fact that the feasible search space is now larger, as the agent now has more choices of tours it can take. In all these plots we again observe that MICP-GCS vastly outperforms the MICP, both in terms of runtime as well as %

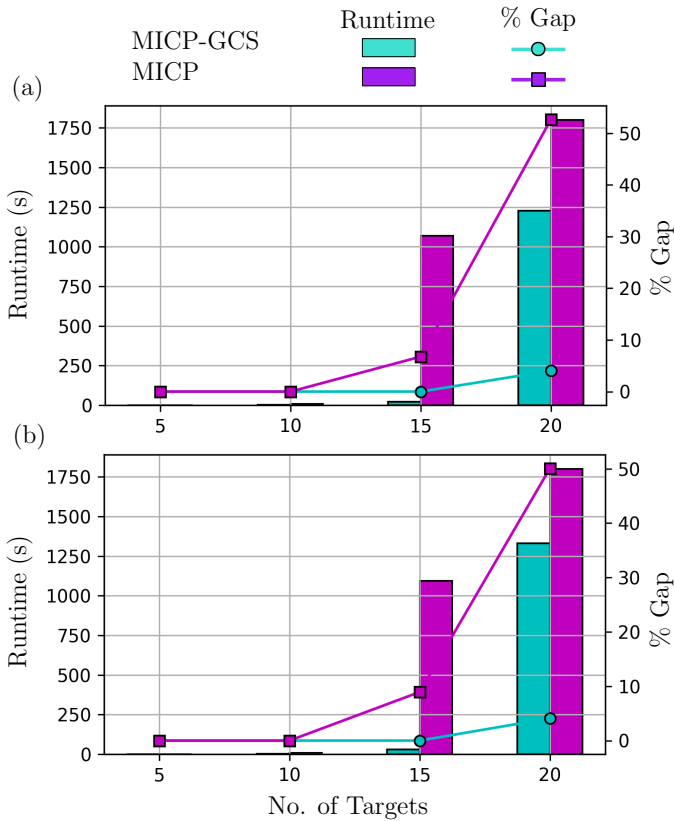


Fig. 4. Numerical results comparing runtime and % Gap of the MICP and MICP-GCS for a fixed time-window duration of 50, and varying max agent speeds of 6 (a), and 8 (b). The plots are very similar to the max agent speed of 4 plot (Fig. 3 (b)). Hence, here too, MICP-GCS gives two orders of magnitude faster runtime with a % Gap improvement of close to 10 for 15 targets. For 20 targets, MICP-GCS is still several hundreds of seconds faster, and gives a % Gap improvement of around 45.

Gap, for 15 and 20 targets.

E. Evaluating the Convex Relaxations

In this section, we evaluate the lower-bounds to the MT-TSP obtained from the convex relaxations of both the MICP and MICP-GCS formulations. To do this, we use ratio, and runtime, which we will now explain. Given an agent max speed, a time-window duration, and the formulation of choice, the binary constraints are first relaxed, and the solver is run on all the 20 instances corresponding to a given number of targets. Ratio is then obtained by finding the ratio of the best bound output by the solver, and the best bound output by MICP-GCS previously when the binary constraints were not relaxed, for all these instances, and then finding the average of these values. Runtime is obtained by finding the average of the solver runtime for all these instances. Note that a higher ratio is always better as it shows that the convex relaxation provides tight lower-bounds comparable to the ones from MICP-GCS with binary constraints. The worst ratio achievable is 0, indicating a trivial lower-bound from the convex relaxation. The ratios and runtimes found are summarized in Table I, and Table II respectively.

Expr	5 Tar	10 Tar	15 Tar	20 Tar
Tw25	0.95	0.82	0.77	0.68
Tw50	0.78	0.63	0.61	0.54
Tw75	0.66	0.56	0.48	0.54
Spd6	0.77	0.65	0.61	0.53
Spd8	0.77	0.65	0.61	0.54

TABLE I

NUMERICAL RESULTS PRESENTING THE RATIOS OBTAINED FROM RELAXED MICP-GCS FOR DIFFERENT EXPERIMENT SETTINGS, AND NUMBER OF TARGETS. WE DO NOT INCLUDE THE RATIOS FOR RELAXED MICP HERE, SINCE THEY WERE ALWAYS THE WORST VALUE OF 0. THE RATIOS GET WORSE WITH MORE TARGETS, AND LARGER TIME-WINDOWS. VARYING THE AGENT SPEED HAS NEGLIGIBLE EFFECT ON THE RATIO.

Expr	5 Tar	10 Tar	15 Tar	20 Tar
Tw25	0.01 (0.0)	0.03 (0.02)	0.06 (0.04)	0.12 (0.02)
Tw50	0.01 (0.0)	0.02 (0.02)	0.04 (0.04)	0.08 (0.02)
Tw75	0.01 (0.0)	0.01 (0.02)	0.04 (0.06)	0.07 (0.03)
Spd6	0.0 (0.0)	0.01 (0.02)	0.03 (0.04)	0.08 (0.02)
Spd8	0.01 (0.0)	0.01 (0.02)	0.03 (0.04)	0.08 (0.02)

TABLE II

NUMERICAL RESULTS PRESENTING THE RUNTIMES FOR BOTH THE RELAXED MICP-GCS, AND RELAXED MICP (IN PARENTHESES) FOR DIFFERENT EXPERIMENT SETTINGS, AND NUMBER OF TARGETS. THE RUNTIMES INCREASE SLIGHTLY WITH MORE TARGETS, BUT ARE OVERALL NEGLIGIBLE FOR BOTH FORMULATIONS.

In both the tables, the column `Expr` represents the experiment settings, and specifies the various choices of agent speed and time-window duration. Here, `Tw25`, `Tw50`, and `Tw75` represent the same experiment settings used for Fig. 3, where the agent max speed was set at 4, and the time-window duration was varied to be 25, 50, and 75 respectively. Similarly, `Spd6` and `Spd8` represent the experiment settings used for Fig. 4, where the time-window duration was fixed at 50, and the agent max speed was varied to be 6 and 8.

In Table I, we only provide the ratios corresponding to the convex relaxation of MICP-GCS. This is because when relaxed, the MICP always gave the worst bound of 0. This is to be expected, since this formulation relies heavily on big- M constraints. Observe how the lower-bounds from relaxed MICP-GCS is affected by the number of targets and the time-window durations, but not from the varying agent speed. This is consistent with our previous observations. Although the lower-bounds to the MT-TSP are somewhat crude here, especially with larger number of targets and bigger time-windows, the main advantage of relaxing MICP-GCS comes from its negligible runtimes as seen in Table II. Observe that the runtimes from relaxed MICP-GCS are similar to the ones from the relaxed MICP (values within parentheses), but provides significantly stronger lower-bounds to the MT-TSP.

VI. CONCLUSION AND FUTURE WORK

In this paper, we introduced a Mixed Integer Conic Program based on the graph of convex sets (MICP-GCS), that finds the optimum to a special case of the Moving-Target Traveling Salesman Problem where targets move along lines with constant speeds. We proved the validity of this new formulation,

and presented numerical results to corroborate its performance. We showed how our MICP-GCS outperforms the current state-of-the-art MICP across various experiments, and also how the MICP-GCS has a much stronger convex relaxation than the baseline MICP. For future work, we plan on investigating how a similar approach presented in this paper can be used to solve a more generalized problem where static obstacles are present.

REFERENCES

- [1] P. Oberlin, S. Rathinam, and S. Darbha, "Today's traveling salesman problem," *IEEE robotics & automation magazine*, vol. 17, no. 4, pp. 70–77, 2010.
- [2] Y. Liu and R. Bucknall, "Efficient multi-task allocation and path planning for unmanned surface vehicle in support of ocean operations," *Neurocomputing*, vol. 275, pp. 1550–1566, 2018.
- [3] J. L. Ryan, T. G. Bailey, J. T. Moore, and W. B. Carlton, "Reactive tabu search in unmanned aerial reconnaissance simulations," in *1998 Winter Simulation Conference. Proceedings (Cat. No. 98CH36274)*, vol. 1, pp. 873–879, IEEE, 1998.
- [4] Z. Yu, L. Jinhai, G. Guochang, Z. Rubo, and Y. Haiyan, "An implementation of evolutionary computation for path planning of cooperative mobile robots," in *Proceedings of the 4th World Congress on Intelligent Control and Automation (Cat. No. 02EX527)*, vol. 3, pp. 1798–1802, IEEE, 2002.
- [5] A. M. Ham, "Integrated scheduling of m-truck, m-drone, and m-depot constrained by time-window, drop-pickup, and m-visit using constraint programming," *Transportation Research Part C: Emerging Technologies*, vol. 91, pp. 1–14, 2018.
- [6] S. Venkatachalam, K. Sundar, and S. Rathinam, "A two-stage approach for routing multiple unmanned aerial vehicles with stochastic fuel consumption," *Sensors*, vol. 18, no. 11, p. 3756, 2018.
- [7] H. A. Saleh and R. Chelouah, "The design of the global navigation satellite system surveying networks using genetic algorithms," *Engineering Applications of Artificial Intelligence*, vol. 17, no. 1, pp. 111–122, 2004.
- [8] O. Cheikhrouhou, A. Koubâa, and A. Zarrad, "A cloud based disaster management system," *Journal of Sensor and Actuator Networks*, vol. 9, no. 1, p. 6, 2020.
- [9] J. Conesa-Muñoz, G. Pajares, and A. Ribeiro, "Mix-opt: A new route operator for optimal coverage path planning for a fleet in an agricultural environment," *Expert Systems with Applications*, vol. 54, pp. 364–378, 2016.
- [10] W. Zhao, Q. Meng, and P. W. Chung, "A heuristic distributed task allocation method for multivehicle multitask problems and its application to search and rescue scenario," *IEEE transactions on cybernetics*, vol. 46, no. 4, pp. 902–915, 2015.
- [11] B. L. Brumitt and A. Stentz, "Dynamic mission planning for multiple mobile robots," in *Proceedings of IEEE International Conference on Robotics and Automation*, vol. 3, pp. 2396–2401, IEEE, 1996.
- [12] C. S. Helvig, G. Robins, and A. Zelikovsky, "The moving-target traveling salesman problem," *Journal of Algorithms*, vol. 49, no. 1, pp. 153–174, 2003.
- [13] C. D. Smith, "Assessment of genetic algorithm based assignment strategies for unmanned systems using the multiple traveling salesman problem with moving targets," 2021.
- [14] A. Stieber and A. Fügenschuh, "Dealing with time in the multiple traveling salespersons problem with moving targets," *Central European Journal of Operations Research*, vol. 30, no. 3, pp. 991–1017, 2022.
- [15] R. S. de Moraes and E. P. de Freitas, "Experimental analysis of heuristic solutions for the moving target traveling salesman problem applied to a moving targets monitoring system," *Expert Systems with Applications*, vol. 136, pp. 392–409, 2019.
- [16] Y. Wang and N. Wang, "Moving-target travelling salesman problem for a helicopter patrolling suspicious boats in antipiracy escort operations," *Expert Systems with Applications*, vol. 213, p. 118986, 2023.
- [17] D. Marlow, P. Kilby, and G. Mercer, "The travelling salesman problem in maritime surveillance—techniques, algorithms and analysis," in *Proceedings of the international congress on modelling and simulation*, pp. 684–690, 2007.
- [18] A. Maskooki and M. Kallio, "A bi-criteria moving-target travelling salesman problem under uncertainty," *European Journal of Operational Research*, 2023.
- [19] B. Englot, T. Sahai, and I. Cohen, "Efficient tracking and pursuit of moving targets by heuristic solution of the traveling salesman problem," in *52nd IEEE conference on decision and control*, pp. 3433–3438, IEEE, 2013.
- [20] P. Chalasani and R. Motwani, "Approximating capacitated routing and delivery problems," *SIAM Journal on Computing*, vol. 28, no. 6, pp. 2133–2149, 1999.
- [21] M. Hammar and B. J. Nilsson, "Approximation results for kinetic variants of tsp," in *Automata, Languages and Programming: 26th International Colloquium, ICALP'99 Prague, Czech Republic, July 11–15, 1999 Proceedings* 26, pp. 392–401, Springer, 1999.
- [22] M. Hassoun, S. Shoval, E. Simchon, and L. Yedidsion, "The single line moving target traveling salesman problem with release times," *Annals of Operations Research*, vol. 289, pp. 449–458, 2020.
- [23] J.-M. Bourjolly, O. Gurtuna, and A. Lyngvi, "On-orbit servicing: a time-dependent, moving-target traveling salesman problem," *International Transactions in Operational Research*, vol. 13, no. 5, pp. 461–481, 2006.
- [24] N. S. Choubey, "Moving target travelling salesman problem using genetic algorithm," *International Journal of Computer Applications*, vol. 70, no. 2, 2013.
- [25] C. Groba, A. Sartal, and X. H. Vázquez, "Solving the dynamic traveling salesman problem using a genetic algorithm with trajectory prediction: An application to fish aggregating devices," *Computers & Operations Research*, vol. 56, pp. 22–32, 2015.
- [26] Q. Jiang, R. Sarker, and H. Abbass, "Tracking moving targets and the non-stationary traveling salesman problem," *Complexity International*, vol. 11, no. 2005, pp. 171–179, 2005.
- [27] U. Ucar and S. K. İşleyen, "A meta-heuristic solution approach for the destruction of moving targets through air operations.," *International Journal of Industrial Engineering*, vol. 26, no. 6, 2019.
- [28] T. Marucci, J. Umenberger, P. Parrilo, and R. Tedrake, "Shortest paths in graphs of convex sets," *SIAM Journal on Optimization*, vol. 34, no. 1, pp. 507–532, 2024.